Non-Invasive Monitoring of Knee Osteoarthritis Severity Using Vibration Stimulation

Takeshi Tokoshima[1], Kazunori Hase[1], Rui Gong[2,*], Makoto Yoshida[1]

[1]Department of Mechanical Systems Engineering, Tokyo Metropolitan University, Tokyo, Japan

[2]Tokyo Metropolitan Institute for Geriatrics and Gerontology, Tokyo, Japan

Received 01 August 2024; received in revised form 11 October 2024; accepted 14 October 2024.

DOI: https://doi.org/10.46604/peti.2024.14079

Abstract

This study aims to explore the application of vibration stimulation for the early detection and assessment of knee osteoarthritis severity, using a porcine knee joint. Accelerometers are attached to the femurs and tibias to measure vibratory responses under simulated osteoarthritic conditions. Frequency response functions are generated from the acceleration data and quantified using the root mean square deviation (RMSD) relative to baseline conditions. To ensure the reliability of the results, a coherence filter is applied, confirming significant differences across various stages of joint injury. The RMSD analysis demonstrates the technique's ability to detect phase differences, particularly within the 1000 Hz frequency range. These findings suggest that vibration stimulation could be a feasible non-invasive diagnostic method for assessing osteoarthritis severity in humans. This study highlights the potential of vibration-based diagnostics as an innovative approach for the early detection of osteoarthritis.

Keywords: non-invasive monitoring, frequency response function, knee osteoarthritis, vibration stimulation

1. Introduction

Currently, osteoarthritis affects more than 300 million people worldwide and is one of the most common arthropathies in Japan and Asia [1]. Osteoarthritis affects all joints in the body, including the knee joint, hip joint, and spine. Pain and other symptoms significantly impact patients' daily living activities, health span, and life expectancy. It is also the leading cause of patients requiring long-term care, resulting in significant social and economic burdens.

The knee is the most commonly affected joint, and the prevalence of knee osteoarthritis is anticipated to rise globally as the population ages [1]. Knee osteoarthritis is characterized by pain and abnormal load distribution to the knee joint. In severe cases, biomechanical changes can lead to difficulties in walking. Consequently, many patients with advanced osteoarthritis opt for knee joint replacement surgery, in which the natural joint is replaced with an artificial joint. The global knee joint replacement market is projected to reach 10.34 billion USD by 2022 [2]. The diagnosis of knee osteoarthritis typically involves assessing the severity of the condition using X-rays or magnetic resonance imaging (MRI) [3].

X-rays do not provide sufficient visualization of the cartilage to accurately diagnose the severity of knee osteoarthritis. However, MRI is expensive, time-consuming, and requires access to specialized, large-scale precision equipment and skilled professionals. Additionally, although MRI scans provide detailed observation of lesions and tissue changes, they are typically performed only after the symptoms have advanced, complicating early detection of the disease. Early detection of knee osteoarthritis, especially in mild cases, is crucial for preventing disease progression.

* Corresponding. E-mail address: gong@tmig.or.jp

English language proofreader: Si-Yu Lin

For this purpose, non-invasive, easy-to-use diagnostic equipment that is not time-consuming or expensive and can be used regardless of location or expertise is desired. As an alternative approach, various researchers have investigated the vibrations associated with joint sounds, often referred to as joint acoustic emissions or vibroarthrography [4]. Joint sound analysis provides a non-invasive diagnostic method with the potential for integration into wearable devices [5]. This technique has demonstrated success in diagnosing knee osteoarthritis, showing a strong correlation with traditional imaging methods such as MRI and X-rays [6-7]. Additionally, recent studies have shown that certain knee injuries, such as meniscal tears, can be distinguished from healthy knees by analyzing the acoustic emissions produced by the joint [8-9].

Despite their diagnostic potential, current joint sound analysis techniques are limited in assessing the severity of joint damage. These limitations stem from the restricted frequency and amplitude of vibrations or sounds generated by tissue friction, which may hinder the ability to provide a comprehensive assessment regarding the extent of damage [4]. This highlights the importance of introducing an external source of sound or vibration. For instance, the effect of frequency on the detection of meniscal damage or tears has been confirmed using vibration stimuli [9]. In other words, it may be feasible to estimate the severity of knee osteoarthritis through vibration stimulation of the knee, rather than relying solely on joint sounds produced during movement.

This study aims to determine the impact of knee osteoarthritis, including contributing factors such as meniscal injury and cartilage softening (an early manifestation of the disease), on the frequency response functions (FRFs). To accurately diagnose the severity of knee osteoarthritis using these non-invasive methods, examining knees with varying degrees of degeneration is necessary. Therefore, porcine legs which share anatomical similarities with human knees are used as subjects. This approach enables reliable and cost-effective studies, maximizing the validity of the proposed method, which is commonly employed in certain medical devices and treatments [10]. Additionally, a frequency spectrum analysis of the porcine knee joint based on vibration stimulation is conducted to evaluate its ability to detect structural changes. External vibrations are applied to measure the knee joint's transmissibility at different stages of damage, and the resulting FRF data are analyzed to identify injuries. This study hypothesizes that significant differences and effect sizes will be more pronounced at certain injury stages than at other stages, similar to previous studies that detected meniscal injuries.

2. Methodology

Before describing the methodology, it is essential to explain certain symbols and definitions to facilitate understanding of the subsequent methodology and equations. A_{in} and A_{out} : These represent the acceleration (A) signals, classified according to the position of the installed accelerometer. One accelerometer is placed just above the patella on the femoral side (denoted as ‘in’) and another on the tibial rough surface (denoted as ‘out’). A'_{in} and A'_{out} : These denote the noise-removed forms of the acceleration signals A_{in} and A_{out}. $F_{Initial}$ and F_{Injury} : These represent the FRFs used in the frequency response analysis. The FRF includes seven damage states for both gain and phase. In this study, the initial state is considered the baseline, and the injury states are collectively referred to as " injured " when expressed in the general formula. f : This denotes the frequency. Because it is digital, it is an integer. The frequency resolution is set to 10 Hz and is expressed as the root mean square deviation (RMSD). f_c : This denotes the frequency center, which is the midpoint of the frequency span. f_b : This represents the frequency band and the length of one side of the span from the center of the frequency span.

H_1, H_2, and H_v : These estimators are used when performing FRF. H_1 is used to eliminate noise, H_2 is used when noise is mixed with the signal on the output side, and H_v is used when noise is mixed with the signal on the input side, and when both sides have mixed noise. N : This represents the time required to calculate the power spectrum. t : This denotes time. W_{in} and W_{out} : These represent the power spectral density of the acceleration A_{in} and A_{out}. $X_{in\text{-}out}$: This represents the cross-spectrum density. Y : This represents the Fourier transform of the time-series acceleration. r^2 : This denotes the coherence function that represents the correlation between the input and output signals.

Structural health monitoring, which is widely used to estimate the state of internal injuries in mechanical structures, has also been commonly applied to biological tissues. Some studies have estimated the injury states using a single-sensor arrangement [11]. This approach is employed to investigate the internal knee structure of a porcine leg. This approach allowed for experiments and analysis of the injury state using a simple structure with only two accelerometer arrangements: input and output.

Acceleration signals measured at a sampling frequency of 1 MHz are first filtered using an infinite impulse response (IIR) bandpass filter with a frequency range of 20-3000 Hz to remove unwanted frequency components (noise). The bandpass filter uses a Kaiser window with a steepness of 1. The overlap is set to 10%, and the signal is time-averaged. Next, for the input and output FRF of acceleration, an estimator Hv is used to account for the noise from both accelerometers [Eqs. (1)-(4)] [12], because the two accelerometers serve as the input and output signals. Using this method, the noise in the input and output measurement signals can be eliminated. The coherence, which indicates the reliability and consistency of the response in the frequency domain, is also calculated [Eq. (5)]. The motivation for this step is that by analyzing the FRF, the relationship between the input signal (excitation) and output signal (response) can be understood, providing a foundation for subsequent damage assessment.

Next, the RMSD (in dB) is used to quantify the differences in the FRF across injury states. The baseline is calculated after transforming the FRF into a frequency span matrix with frequency center f_c and frequency band f_b to identify the different parts of the FRF results obtained at various stages of knee injury as shown in Eq. (6) [13]. Similarly, the coherence function is converted into a matrix and applied as a coherence filter, making all FRFs with a coherence below 0.5 per f_c and f_b excluded from the RMSD calculation. In this process, the coherence matrix and coherence filtering are used to assess the reliability of the FRF data and to screen for reliable frequency ranges.

$$Y(f) = \sum_{t=1}^{N} A(t) exp\left(-\frac{2\pi i}{N}(t-1)(f-1)\right) \tag{1}$$

$$W = \left|\frac{Y(f)}{N}\right|^2 \frac{1}{\Delta f} \tag{2}$$

$$X = Y_{in}(f)^* Y_{out}(f) \tag{3}$$

$$H_v = \sqrt{H_1} \bullet \sqrt{H_2} = \sqrt{\frac{\overline{X_{in-out}(f)}}{\overline{W_{in}(f)}}} \sqrt{\frac{\overline{W_{out}(f)}}{\overline{X_{in-out}(f)^*}}} = \sqrt{\frac{\overline{W_{out}(f)}}{\overline{W_{in}(f)}}} \frac{W_{in-out}(f)}{|W_{in-out}(f)|} \tag{4}$$

$$\gamma^2(f) = \frac{\left|\overline{X_{in-out}(f)}\right|^2}{\overline{W_{in}(f)}\,\overline{W_{out}(f)}} \qquad \left(0 \le \gamma^2 \le 1\right) \tag{5}$$

$$RMSD(f_c, f_b) = \sqrt{\frac{\sum_{f=f_c-f_b}^{f=f_c+f_b} \left\{FRF_{Injured}(f) - FRF_{Initial}(f)\right\}^2}{\sum_{f=f_c-f_b}^{f=f_c+f_b} FRF_{Initial}(f)^2}} \tag{6}$$

The center frequency f_c is varied from 30 to 2990 Hz in 10-Hz increments, and the frequency band. f_b is examined from 10 to 1510 Hz in 10-Hz increments. The resulting RMSD matrix is first checked for normality using the Kolmogorov-Smirnov test on six samples [14]. Next, two RMSDs at different injury stages are compared using a two-sample technical test (t-test) to identify significantly different frequency spans. Within the frequency range of statistical significance, effect sizes are calculated using Cohen's difference (Cohen's d) to identify regions with large effects [15]. This method is selected because it

enables a comprehensive study, as it is expected to characterize not only a single frequency but also the average of a wide range of frequencies. The RMSD values in the selected frequency range can be considered as characteristics of the internal structural changes in the knee, that is, the occurrence and severity of injury (categorized as healthy, damaged, or lost). Additionally, the coherence of the FRF serves as an indicator of injury severity.

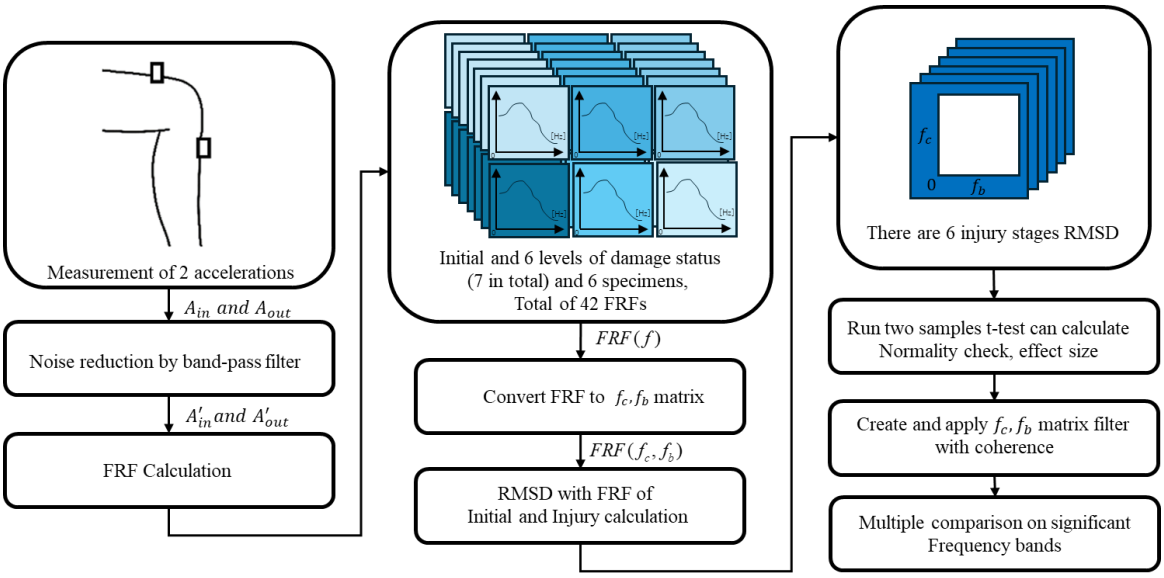

Fig. 1 Signal processing and feature extraction diagram

Furthermore, the FRF coherence is transformed into a frequency span matrix of f_c and f_b, and filtered at frequency spans above a threshold of 0.5 [16]. Although this is a unique approach, it is used to determine reliable data for frequency analysis. Finally, a multiple comparison test (Fisher's least significant difference method) is applied to the feature portions with large effect sizes to confirm that they are not influenced by the experimental environment [17]. The series of analysis flows are summarized in Fig. 1.

3. Experiments

Based on the above methodology, this study aims to design a system to detect the effects of changes in the internal knee structure on the FRF. A porcine leg is prepared as a specimen and placed in the experimental apparatus. Next, an instrument is attached to transmit vibrations to the knee using a shaker. The knee is injured, and the same experiment is performed. The obtained acceleration signals are analyzed. The process is described in detail in the following subsections.

3.1. Specimen preparation

Six frozen porcine hind legs, each from a 2-year-old pig, are obtained from Tokyo Shibaura Organ Co. Before the experiments, the legs are thawed in a 20°C water bath for 12 h. Unnecessary parts are then removed to simulate the appearance of a human knee while avoiding damage to the tissues surrounding the knee. Manual flexion-extension exercises are carefully performed on each leg prior to data collection to ensure full thawing.

3.2. Injury simulation

In this study, seven testing stages are considered to mimic the severity of knee osteoarthritis: initial, soft tissue damage, meniscus injury, meniscus tear, cartilage softening, cartilage injury, and cartilage loss. The testing stages are summarized in Fig. 2. The seven test phases include meniscal injury, which causes knee osteoarthritis; cartilage softening, which is an early symptom of osteoarthritis; and cartilage injury leading to cartilage loss. The first measurement is performed on a knee with a complete internal structure and the data are used as references [Fig. 3(a)].

Next, an incision is made in the soft tissue (deep into the synovial membrane) without damaging the internal structures, and the meniscus and other structures are operated upon until they are visible [Fig. 3(b)]. The meniscus is then slightly cut with a scalpel to simulate meniscal contusion [Fig. 3(c)]. Subsequently, the meniscus is cut further using a scalpel to simulate a meniscal tear [Fig. 3(d)]. Care is taken not to touch the anterior or posterior cruciate ligaments. Next, papain solution is applied to simulate cartilage softening [Fig. 3(e)]. The papain solution is prepared by activating freeze-dried papain (Papain, Worthington Biochemical Corporation, USA) at a concentration of 5%. The papain is allowed to react for 1 hour at room temperature. Next, to simulate cartilage wear, incisions are made in the cartilage on both the femoral and tibial sides to provide the appearance of furrows [Fig. 3(f)]. This is performed on the entire surface, with particular attention paid to the points where the load is applied. This condition is grade III in the Kellgren-Lawrence (KL) classification [18]. Finally, all cartilage on both the femoral and tibial sides is removed [Fig. 3(g)].

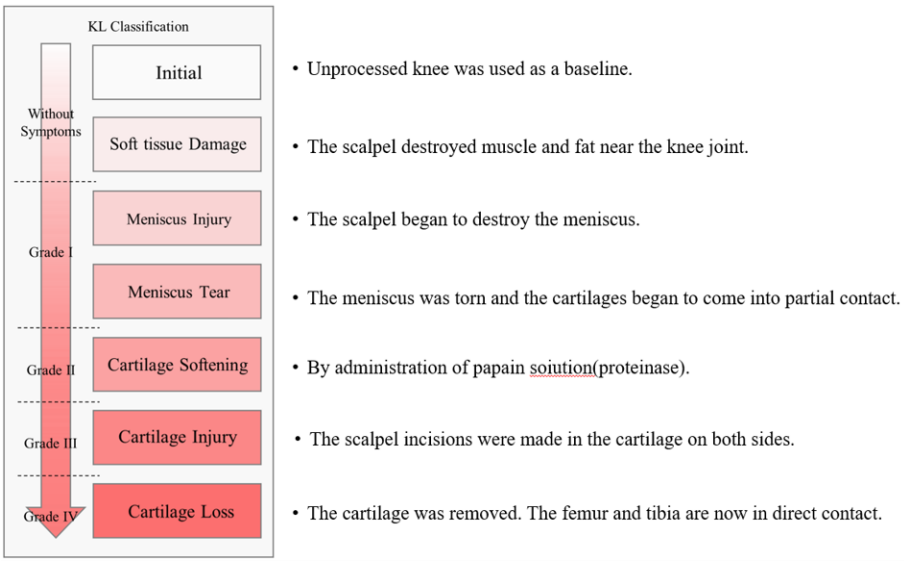

Fig. 2 Steps in injury simulation using porcine legs

It should be noted that the KL classification is a criterion for assessing the severity of knee osteoarthritis based on the joint space visible on radiographs. Meniscal injuries and tears do not significantly affect the joint space observed on radiographs. Consequently, a one-to-one correspondence between the KL classification and the processing flow is illustrated in Fig. 2. Additional information for each damage phase simulation is provided on the right side of the figure.

(a) Initial status

(b) Soft tissue damage

(c) Meniscus injury

(d) Meniscus tear

(e) Cartilage softening

(f) Cartilage injury

(g) Cartilage loss

Fig. 3 Appearance of porcine leg injury simulation

Fig. 3 shows a macroscopic view of the simulated injury and degeneration of the porcine leg. However, because the primary damaged areas are the cartilage and meniscus, a schematic of the coronal plane is necessary to further illustrate how knee injury or degeneration can be simulated. To aid in understanding, Figs. 3 and 4 present a simplified version of the typical geometry of a porcine knee, showing the femur, tibia, cartilage, meniscus, and soft tissues surrounding the entire knee joint.

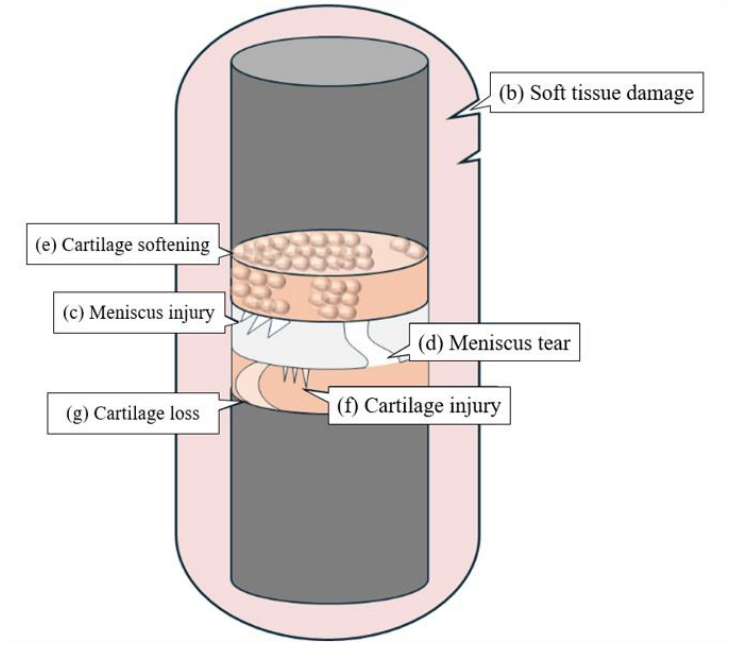

Fig. 4 A schematic illustrating the damage simulation inside the porcine knee

3.3 Vibration test setup

To test the vibration of the porcine legs, the legs are placed on a stand that simulates a human sitting position, with the knees bent at 90° (Fig. 5). The sample is placed on a vibration absorption pad on the contact surface to isolate the vibration system from the external environment. Vibrations are applied to the femoral condyles using an inertial shaker (Model 2002E, Modal Shop Inc., Cincinnati, USA). The magnitude of the vibration is 2 V on an oscilloscope (PicoScope 4824A, Pico Technology Ltd., Cambridgeshire, UK), the swept sine signal is incremented by 3 Hz/ms, and the sweep bandwidth is 20-3000 Hz. A uniaxial accelerometer (353B16, PCB Piezotronics, Inc., New York, USA) with a sampling frequency of 1 MHz is placed on the patella and rough tibial surface. The accelerometer is installed with its axis perpendicular to the knee cartilage. The accelerometer and porcine leg are secured with a proprietary belt and adjusted so that a load of 5 N is applied to the contact points. Accelerometer signals are processed with a sensor signal conditioner (482C05, PCB Piezotronics, Inc., New York, USA), and are measured with an oscilloscope and received using a PC application (Picoscope 7, Pico Technology Ltd., Cambridgeshire, UK). Oscillations are applied for 50 seconds at a time. The ethics review board of Tokyo Metropolitan University approved the study design (approval number H5-55).

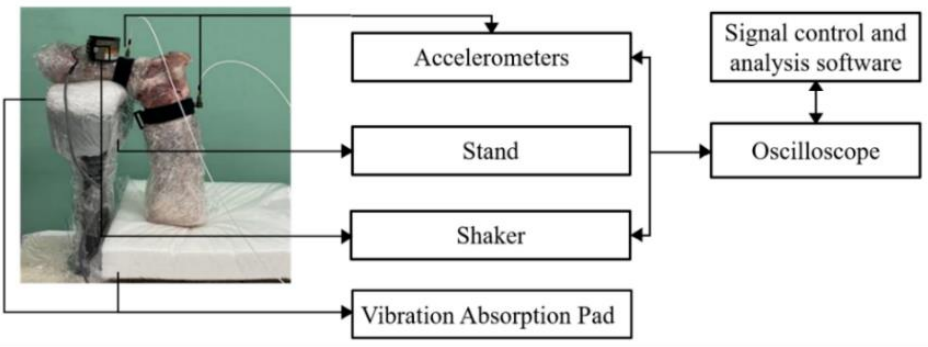

Fig. 5 Porcine knee vibration stimulation setup

4. Results

In the comprehensive analysis of the RMSDs for both the gain and phase, a meticulous comparison is performed between two specific injury stages among the six identified. As illustrated in Fig. 6, the examination focused on the effect size of the phase in the meniscal tear relative to the soft tissue damage.

Notably, the study's selected frequency range (100-1300 Hz) aligns with the parameters used in previous investigations. Among the frequency bands that exhibited significant differences in the two-sample t-test, the application of the coherence filter highlighted a specific band from 560 to 580 Hz with the largest effect size. This frequency span is narrower than those reported in previous studies. The remaining spans are eliminated using a coherence filter. Emphasizing the importance of coherence in the analysis of biological vibration stimulation, this study showed that the coherence filter excludes the entire range of effect sizes, and thus, may be limited in assessing specific injury stages.

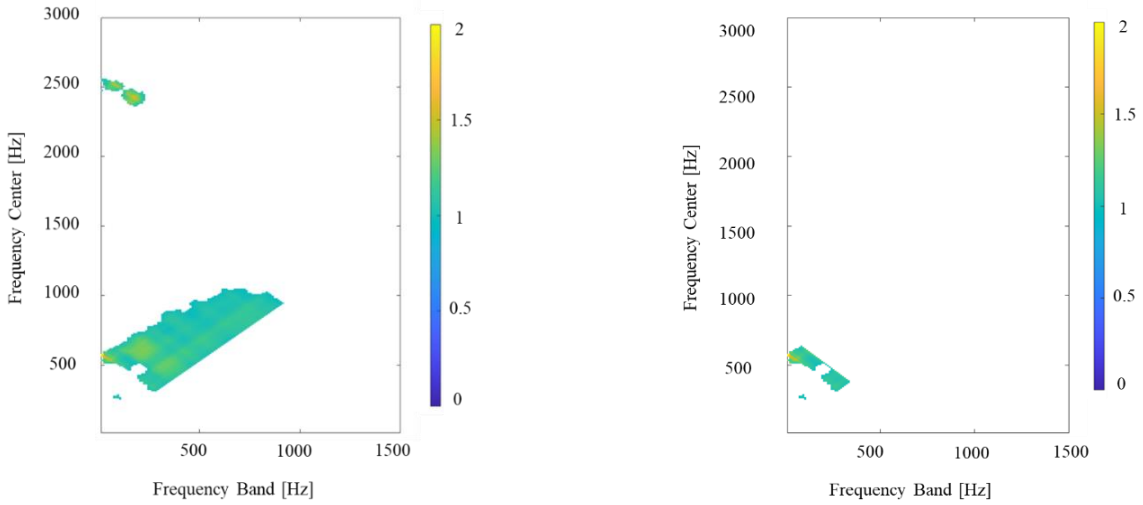

(a) Without coherence filter

(b) Coherence filter applied; areas of two-sample t-test with no significant difference are transparent

Fig. 6 Effect size for each frequency band

Tables 1 and 2 succinctly demonstrate all the results obtained, highlighting the unexpectedly robust effect sizes for most phases. In the tables, the values represent the effect sizes and are unitless. The rows and columns represent the compared damage stages. Cells corresponding to the same damage stage are left blank because only different stages are compared. There are two possible combinations of different damage stages; however, only one is shown because the effect size is expressed as an absolute value. Comparisons for which the two-sample t-test and coherence filter eliminated the evaluable range are denoted by "-". Significant figures are set to decimal places.

Table 1 Maximum gain effect across frequency bands

effect size (-) f_b (Hz)	soft tissue damage	meniscus injury	meniscus tear	cartilage softening	cartilage injury	cartilage loss
soft tissue damage		-	1.19 [500-600Hz]	1.03 [370-390Hz]	1.12 [500-540Hz]	1.43 [750-830Hz]
meniscus injury			1.28 [290-310Hz]	-	1.20 [500-540Hz]	1.29 [500-600Hz]
meniscus tear				1.18 [360-400Hz]	1.43 [420-520Hz]	1.35 [760-900Hz]
cartilage softening					1.12 [380-420Hz]	1.41 [750-830Hz]
cartilage injury						-
cartilage loss						

The results in the tables show that, even in instances where certain ranges are lost (except when all evaluable ranges are lost), effect sizes consistently surpassed the 0.8 threshold, underscoring a substantial effect between the various injury stages [19]. The frequency band f_b ranged from 10 Hz to 430 Hz, showing the spectrum of the strongest effect size frequency bands that varied across different phases. Notably, for frequency spans associated with meniscal injury, cartilage loss, and cartilage softening, cartilage injury presented wider bands, while others generally featured $f_b < 100$ Hz.

Table 2 Maximum phase effect across frequency bands

effect size (-) f_b (Hz)	soft tissue damage	meniscus injury	meniscus tear	cartilage softening	cartilage injury	cartilage loss
soft tissue damage		1.30 [90-110Hz]	2.23 [560-580Hz]	1.70 [570-590Hz]	1.94 [850-890Hz]	2.15 [810-850Hz]
meniscus injury			1.22 [540-580Hz]	-	1.50 [50-730Hz]	1.41 [50-910Hz]
meniscus tear				-	-	1.55 [780-880Hz]
cartilage softening					1.04 [140-820Hz]	1.84 [820-840Hz]
cartilage injury						1.31 [50-690Hz]
cartilage loss						

5. Discussion

Based on the above results, further analysis is conducted. Fig. 6 compares soft tissue damage and meniscal tears. The meniscus is responsible for absorbing and dispersing pressure and shock from the foot. However, in terms of gain, the overall vibration is no longer absorbed as the injury stage progresses. Which aligns with the hypothesis. In Fig. 6, the phase is shown as an example, indicating that the speed of the vibration transmission also showed a significant change. This trend is true for all combinations that exhibited noteworthy differences, suggesting that articular cartilage, including the meniscus, may have partially delayed and dispersed the frequency of the impact, in addition to absorbing the magnitude of the impact itself. Related studies have also confirmed that viscoelastic materials can disperse vibrations in the frequency range, wherein the cartilage and meniscus are typical viscoelastic objects [20].

Another possible cause of the bandwidth eliminated by the coherence filter is insufficient power in the sweep vibration. If the force of the shaker is increased, there is a high possibility that the coherence filter will improve; allowing for evaluation over a wider frequency range. Because the coherence filter still has a bandwidth in which the effect can be evaluated, the current excitation force is deemed appropriate. Conversely, the original concept of the coherence filter is considered to have yielded good results, considering that only frequencies below 1000 Hz remained credible under the conditions of this experiment.

A comparison of the six levels of damage showed that as noted in the results, knee injury could be evaluated with either gain or phase, except in one case. Cartilage softening, an early manifestation of knee osteoarthritis, is challenging to detect using the experimental technique but showed a higher effect size for gain than those for meniscal tears. In other words, early diagnosis of knee osteoarthritis may be possible. Although this study observed changes in the same individual, this approach cannot be applied when considering non-invasive diagnosis in humans, as baseline data cannot be collected before the changes. Moreover, there is potential for classifying subtle differences between FRFs when data from knees at each injury stage are collected. By identifying specific frequency bands with high effect sizes, it may be possible to determine whether the observed differences are attributable to individual variations or are specific to the injury stage.

However, apart from the potential to emerge from this method, several limitations should be acknowledged, particularly regarding the detection of knee osteoarthritis and related meniscal injuries. Despite the notable anatomical and biomechanical similarities between porcine and human knee joints, significant differences in joint size, tissue composition, range of motion,

and biomechanical limits must be considered [10]. Therefore, findings from the porcine model may not be directly applicable to humans without further validation. Moreover, although experiments using porcine knees allow the application of varying vibration wave frequencies and amplitudes with minimal safety concerns, human applications require careful determination of safe and effective parameters. This adds to the complexity and limits the immediate generalizability of the results, emphasizing the need for extensive human testing before clinical use. Additionally, the small sample size of six limits the precision of the findings, and the observed changes are within the same individuals, baseline data from before the onset of injury are unavailable. Further research is needed to determine whether the observed differences across the stages of injury are individual-specific or represent generalizable features. Nonetheless, the identification of characteristic frequency bands for each symptom stage suggests potential applicability for future research.

6. Conclusions

In this study, vibration stimulation was applied to porcine knee joints to simulate structural health monitoring and detect changes associated with knee osteoarthritis. Acceleration data from six porcine knees, captured by accelerometers on the femur and tibia, were analyzed across seven simulated injury stages. The results, converted into RMSDs, revealed significant differences between injury stages, as confirmed by the coherence filter and validated through multiple comparison tests. Despite the small sample size, this approach demonstrates the potential for detecting knee osteoarthritis and meniscal injuries. However, further studies with larger sample sizes are necessary to determine whether the observed differences are individual-specific or consistent across injury stages. Notably, the identification of the characteristic frequency bands for each symptom stage indicates their potential application in future research.

Conflicts of Interest

The authors declare no conflict of interest.

Statement of Ethical Approval

(a) Statement of human rights

For this type of study, a statement of human rights is not required.

(b) Statement on the welfare of animals

All procedures performed in studies involving animals were in accordance with the ethical standards of the Tokyo Metropolitan University or the practice at which the studies were conducted.

Statement of Informed Consent

For this type of study, informed consent is not required.

References

[1] H. Long, Q. Liu, H. Yin, K. Wang, N. Diao, Y. Zhang, et al., “Prevalence Trends of Site-Specific Osteoarthritis from 1990 to 2019: Findings from the Global Burden of Disease Study 2019,” Arthritis Rheumatology, vol. 74, no. 7, pp. 1172-1183, 2022.

[2] SkyQuest, “Global Knee Replacement Market Size, Share, Growth Analysis, By Procedure Type, By Component-Industry Forecast 2024-2031,” https://cn.gii.tw/report/sky1461491-global-knee-replacement-market-size-share-growth.html, accessed on 2024. (In Chinese)

[3] T. Sivakumari and R. Vani, “Performance Analysis of Alexnet for Classification of Knee Osteoarthritis,” NeuroQuantology, vol. 20, no. 19, pp. 1686-1692, 2022.

[4] H. K. Jeong, M. B. Pouyan, D. C. Whittingslow, V. Ganti, and O. T. Inan, “Quantifying the Effects of Increasing Mechanical Stress on Knee Acoustical Emissions Using Unsupervised Graph Mining,” IEEE Transactions on Neural Systems and Rehabilitation Engineering, vol. 26, no. 3, pp. 594-601, 2018.

[5] R. Gong, K. Hase, H. Goto, K. Yoshioka, and S. Ota, "Knee Osteoarthritis Detection based on the Combination of Empirical Mode Decomposition and Wavelet Analysis," Journal of Biomechanical Science and Engineering, vol. 15, no. 3, article no. 20-00017, 2020.

[6] A. Machrowska, R. Karpinski, M. Maciejewski, J. Jonak, and P. Krakowski, "Application of Eemd-Dfa Algorithms and Ann Classification for Detection of Knee Osteoarthritis Using Vibroarthrography," Applied Computer Science, vol.20, no. 2, pp. 90-108, 2024.

[7] R. Karpiński, P. Krakowski, J. Jonak, A. Machrowska, and M. Maciejewski, "Comparison of Selected Classification Methods Based on Machine Learning as a Diagnostic Tool for Knee Joint Cartilage Damage Based on Generated Vibroacoustic Processes," Applied Computer Science, vol. 19, no.4, pp. 136-150, 2023.

[8] C. N. Teague, J. A. Heller, B. N. Nevius, A. M. Carek, S. Mabrouk, F. Garcia-Vicente, et al., "A Wearable, Multimodal Sensing System to Monitor Knee Joint Health," IEEE Sensors Journal, vol. 20, no. 18, pp. 10323-10334, 2020.

[9] M. Safaei, N. B. Bolus, D. C. Whittingslow, H. K. Jeong, A. Erturk, and O. T. Inan, "Vibration Stimulation as a Non-Invasive Approach to Monitor the Severity of Meniscus Tears," IEEE Transactions on Neural Systems and Rehabilitation Engineering, vol. 29, pp. 350-359, 2021.

[10] T. Takroni, L. Laouar, A. Adesida, J. A. W. Elliott, and N. M. Jomha, "Anatomical Study: Comparing the Human, Sheep and Pig Knee Meniscus," Journal of Experimental Orthopaedics, vol. 3, article no. 35, 2016.

[11] A. C. Altunışık, F. Y. Okur, S. Karaca, and V. Kahya, "Vibration-Based Damage Detection in Deam Structures with Multiple Cracks: Modal Curvature vs. Modal Flexibility Methods," Nondestructive Testing and Evaluation, vol. 34, no. 1, pp. 33-53, 2019.

[12] Z. Mao and M. Todd, "Statistical Modeling of Frequency Response Function Estimation for Uncertainty Quantification," Mechanical Systems and Signal Processing, vol. 38, no. 2, pp. 333-345, 2013.

[13] V. Giurgiutiu and A. Zagrai, "Damage Detection in Thin Plates and Aerospace Structures with the Electro-Mechanical Impedance Method," Structural Health Monitoring, vol. 4, no. 2, pp. 99-118, 2005.

[14] G. Marsaglia, W. W. Tsang, and J. Wang, "Evaluating Kolmogorov's Distribution," Journal of Statistical Software, vol. 8, no. 18, pp. 1-4, 2003.

[15] M. E. Rice and G. T. Harris, "Comparing Effect Sizes in Follow-Up Studies: ROC Area, Cohen's d, and r," Law and Human Behavior, vol. 29, no. 5, pp. 615-620, 2005.

[16] J. M. Liu, Y. F. Xu, and W. D. Zhu, "New Coherence Function with Measurements of One Sampling Period," Mechanical Systems and Signal Processing, vol. 88, pp. 354-376, 2017.

[17] U. Meier, "A Note on the Power of Fisher's Least Significant Difference Procedure," Pharmaceutical Statistics, vol. 5, no. 4, pp. 253-263, 2006.

[18] J. H. Kellgren and J. S. Lawrence, "Radiological Assessment of Osteo-Arthrosis," Annals of the Rheumatic Diseases, vol. 16, no. 4, pp. 494-502, 1957.

[19] J. Cohen, Statistical Power Analysis for the Behavioral Sciences, 2nd ed., New Jersey: Lawrence Erlbaum Associates, 1988.

[20] Y. Maximov, Y. Legovich, and D Maximov, "Frequency Characteristics of Viscoelastic Damper Models and Evaluation of a Damper Influence on Induced Oscillations of Mechanical System Elements," Meccanica, vol. 56, pp. 3107-3124, 2021.